Development of a method for determining the impact characteristics of a Masset hammer based on a combined simulation and experimental approach

Mai Duy Phuong*

Institute of Missile, Academy of Military Science and Technology, 17 Hoang Sam, Nghia Do, Hanoi, Vietnam.
*Corresponding author: phuongmd1975@gmail.com
Received 29 Jun. 2026; Revised 16 Aug. 2026; Accepted 04 Sep. 2026; Published 16 Sep. 2026.
DOI: https://doi.org/10.54939/1859-1043.j.mst.FMC.2026.3-10

ABSTRACT

This study proposes a method combining dynamic simulation and experimental impact-force data to quantitatively determine the dynamic characteristics of a Masset hammer throughout the entire operating process, particularly the impact acceleration, which is difficult to determine experimentally. An impulse absorption coefficient, η, is introduced to regulate the relationship between the force measured at the anvil and the actual force acting on the hammer, thereby ensuring that the calculated results are consistent with actual physical conditions. The results show that only a portion of the impact energy is transmitted to the anvil, while the remaining part is dissipated due to the energy-absorption characteristics of the structure; this provides a direct quantitative basis for selecting the test conditions. The proposed method does not require material modeling in the contact region and can be applied to similar hammer systems.

Keywords: Masset hammer; Dynamics; Impact acceleration.

1. INTRODUCTION

In shock resistance tests, reproducing acceleration loads similar to pyroshock is important for evaluating the operational capability of equipment under actual conditions [1, 2]. A Masset hammer is commonly used to generate high-amplitude mechanical shock pulses with very short durations [3, 4]. However, the selection of test conditions is still mainly based on experience or existing technical documents, without an accurate quantitative basis.

During impact, the hammer-head acceleration is the key parameter governing the load applied to the test object, but it is difficult to measure directly because of the short impact duration and the rapidly varying high-amplitude load. In contrast, the impact force at the anvil as a function of time is the most accessible experimental signal. This limitation requires the development of a method to determine the hammer-head acceleration and velocity from measured impact-force data combined with the dynamic state of the system at the moment of impact.

To address this issue, a dynamic model of the cam–hammer–counterweight system is developed to determine the motion state before and during impact. Experimental impact-force data are then incorporated into the rotational dynamic equation to determine the hammer-head acceleration during impact. The proposed method is validated using independent criteria based on fundamental mechanical laws.

2. ROTATIONAL DYNAMIC MODEL

The Masset hammer system is a mechanical system involving rotational, oscillatory, and impact motions. Therefore, to investigate its dynamic behavior, it is necessary to develop an equivalent mechanical model that accounts for all degrees of freedom and dynamic constraints.

2.1. Mechanical system modeling

A Cartesian coordinate system is defined with the origin at the rotation center O, where the O*x* axis is horizontal and the O*y* axis is vertical. The positive direction of torque is counterclockwise. The system consists of two coupled bodies connected by an inextensible belt:

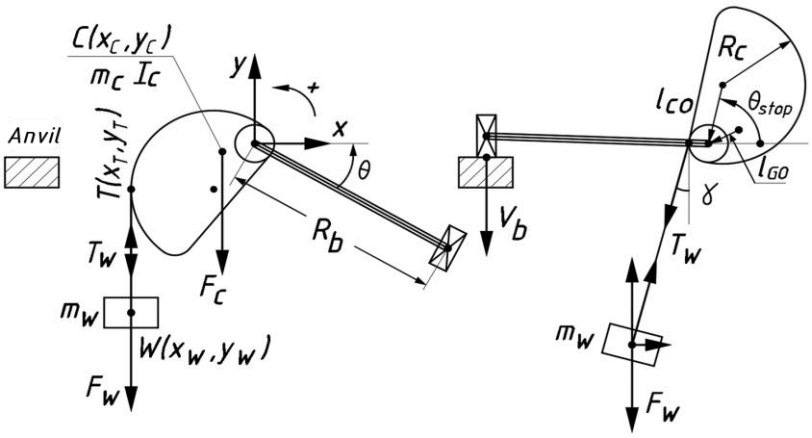


Figure 1. *Mechanical model of the Masset hammer system before and after impact.*

- Rotating body: The cam and hammer (including the test specimen) are modeled as a rigid body rotating about a fixed axis at O. The total mass is m_C, the moment of inertia about its center of mass is I_C, at C(x_C, y_C) and the distance from the center of mass to the rotation axis O is l_{GO}. According to the Steiner theorem, the moment of inertia of the cam about O is given by:

$$I_q = I_C + m_C.l^2_{GO} \quad (1)$$

- Counterweight: A mass mw is attached to the belt and moves freely in the O*xy* plane, with its center of mass located at W(x_W, y_W). The belt tension T_W acts on the counterweight along the direction from W to T.

- Belt: The belt is inextensible, with constant total length L_d, and is wrapped around the cam profile. The coordinates of the contact point (the point where the belt detaches from the cam profile), T(x_T, y_T), depend on the rotation angle θ and the counterweight swing angle γ.

2.2. Geometric modeling of the cam profile

Geometric modeling of the cam profile enables determination of key parameters such as force lever arm, contact radius, and center of mass position as functions of rotation angle θ and counterweight angle γ, while reducing model complexity. The cam shaft is mounted with a toothed ring to adjust the initial hammer angle; more teeth correspond to a larger initial angle. The cam profile consists of two connected circular arcs: a main arc of radius R_C offset from O by l_{CO}, and an inner arc of radius Rtam centered at O. The condition for continuous contact is given by:

$$R_C = l_{CO} + R_{tam} \quad (2)$$

Absolute angle of the cam center measured from the Ox axis:

$$\theta = \theta_0 + \Delta\theta \quad (3)$$

where θ_0 is the initial angle determined by the tooth position, $\Delta\theta$ is the angular displacement from the initial position (an integral variable), and γ is the belt swing angle measured from the negative Oy direction, taken as positive when the belt inclines to the right.

- Phase transition and contact point T: The belt transitions from the R_C arc to the R_{tam} arc when the contact points coincide. Define the phase angle $\varphi = \theta - \gamma$. From (2):

$$\varphi = \theta - \gamma = 0 \quad (4)$$

At $\varphi = 0$, the coordinates of T obtained from both expressions are identical, giving $(-R_{tam}.\cos\gamma, -R_{tam}.\sin\gamma)$:

$\varphi < 0$: belt contacts the R_C arc: $x_T = l_{CO}\cos\theta - R_C\cos\gamma$; $y_T = l_{CO}\sin\theta - R_C\sin\gamma$ (5)

$\varphi \geq 0$: belt contacts the R_{tam} arc: $x_T = -R_{tam}\cos\gamma$; $y_T = -R_{tam}\sin\gamma$ (6)

- The signed moment arm of T_W about O is the projection of OT onto the direction perpendicular to the belt:

$$l_T = x_T \cos\gamma + y_T \sin\gamma \tag{7}$$

Continuity at the transition point ($\varphi = 0$):

Phase 1: $l_{T|\varphi=0} = (l_{CO} - R_C)(cos^2\gamma + sin^2\gamma) = l_{CO} - R_C = -R_{tam}$*.

Phase 2: $l_T = -R_{tam}(cos^2\gamma + sin^2\gamma) = -R_{tam}$*.

Thus, in Phase 2 (belt in contact with the axis), $l_T = -R_{tam}$ is constant and independent of γ.

- The center of mass G and the geometric center C belong to the same rigid body rotating about O. When the cam rotates by an additional angle $\Delta\theta$ from the initial position:

$$x_G = x_{G0}\cos\Delta\theta - y_{G0}\sin\Delta\theta; \quad y_G = x_{G0}\sin\Delta\theta + y_{G0}\cos\Delta\theta \tag{8}$$

where (x_{G0}, y_{G0}) are the coordinates of the center of mass at the initial configuration ($\Delta\theta = 0$), determined from the reference position (hammer-anvil contact) by an inverse rotation.

- L_d is the total belt length. The wrapped belt length depends on the geometric phase and, via Equation (4), on γ:

$\varphi < 0$ (phase 1): $$s = [(\gamma - \theta).R_C + 90.R_{tam}].\pi/180 \tag{9}$$

$\varphi \geq 0$ (phase 2): $$s = [(\gamma - \theta).R_{tam} + 90.R_{tam}].\pi/180 \tag{10}$$

where θ_{stop} is the cam angular position at the hammer–anvil contact point. At the transition point ($\theta = \gamma$), both expressions yield the same result: $s = (\theta_{stop} - \gamma)\cdot R_{tam}\cdot(\pi/180)$, ensuring continuity. When $\theta = \theta_{stop}$ (hammer–anvil impact), $s = 0$ and $l = L_d$ (the entire belt is free). The length of the free belt segment from T to the counterweight W is:

$$l = L_d - s \tag{11}$$

2.3. Equation of motion of the counterweight

The general Newton's equation governing the motion of the counterweight is given by: $m_W.\vec{a}_W = \vec{T}_W + \vec{P}$, Projecting Newton's equation along the belt direction (from W to T) gives:

$$T_W = m_W.(l.\dot{\gamma}^2 + g\cos\gamma - l_{CO}\sin\phi.\omega^2 + l_T.\alpha) \tag{12}$$

and defining $Q = \begin{cases} l.\dot{\gamma}^2 + g\cos\gamma - l_{CO}\sin\phi.\omega^2 & \phi < 0 \text{ (pha 1)} \\ l.\dot{\gamma}^2 + g\cos\gamma & \phi \geq 0 \text{ (pha 2)} \end{cases}$, tension force equation:

$$T_W = m_W.(Q + l_T.\alpha) \tag{13}$$

Projecting Newton's equation along the belt normal gives the acceleration equation:

$$\ddot{\gamma} = \begin{cases} (-g\sin\gamma + l_{CO}\cos\phi.\omega^2 + l_{CO}\sin\phi.\alpha - 2r\omega.\dot{\gamma} + r.\dot{\gamma}^2)/l & \phi < 0 \text{ (phase 1)} \\ (-g\sin\gamma - 2r\omega.\dot{\gamma} + r.\dot{\gamma}^2)/l & \phi \geq 0 \text{ (phase 2)} \end{cases} \tag{14}$$

2.4. Rotational equation of motion of the cam

Applying the moment equation about point O:

$$I_q.\alpha = \Sigma M = M_C + M_W = -m_C.g.x_C - T_W.l_T \tag{15}$$

Moment due to gravity acting at C: $M_C = -m_C.g.x_C$ (the negative sign indicates that when $x_C > 0$, gravity produces a resisting moment opposite to the positive convention). Moment due to belt tension: $M_W = -T_W.l_T$.

2.5. Formulation of the system of differential equations

Equations (12) and (15) contain two unknowns, T_W and α. Substituting T_W from (12) into (15) allows α to be solved as:

$$\alpha = -(m_C.g.x_C + m_W.Q.l_T)/(I_q + m_W.l_T^2) \quad (16)$$

Collecting all transformations, a system of first-order differential equations with four state variables $q = [\Delta\theta, \omega, \gamma, \dot{\gamma}]^T$ is obtained as:

$$\begin{cases} (1)\dfrac{d(\Delta\theta)}{dt} = \omega \qquad (2)\dfrac{d\omega}{dt} = -\dfrac{m_C.g.x_C + m_W Q.l_T}{I_q + m_W l_T^2} \qquad (3)\dfrac{d\gamma}{dt} = \dot{\gamma} \\ (4)\dfrac{d\dot{\gamma}}{dt} = \begin{cases} (-g\sin\gamma + l_{CO}\cos\phi.\omega^2 + l_{CO}\sin\phi.\alpha - 2r\omega.\dot{\gamma} + r.\dot{\gamma}^2)/l & \phi < 0 \text{ (phase 1)} \\ (-g\sin\gamma - 2r\omega.\dot{\gamma} + r.\dot{\gamma}^2)/l & \phi \geq 0 \text{ (phase 2)} \end{cases} \end{cases} \quad (17)$$

T_W and α, given by Equations (12) and (16), are algebraic variables solved explicitly at each time step.

2.6. Impact energy dissipation

In the modeling, the energy losses due to friction and other resistance effects associated with relative motion between system components are assumed to be small compared with the energy transferred within the mechanical system during the impact event, the decrease in potential energy is fully converted into the kinetic energy of the cam and the counterweight:

$$\Delta PE = \Delta KE \quad (18)$$

At the impact instant, the decrease in potential energy is compared with the total kinetic energy of the system to evaluate the conservation error. The system kinetic energy consists of the rotational kinetic energy of the cam and the kinetic energy of the counterweight:

$$KE = (I_q.\omega^2_{vc} + m_W.v^2_W)/2 \quad (19)$$

The counterweight velocity v_W at the moment of impact consists of two components: the tangential component due to the pendulum wire motion $l.\dot{\gamma}$, which continues to exist as the swinging motion of the counterweight, and the radial component caused by the cam rotation $R_{tam}.\omega_{vc}$, which vanishes instantaneously.

$$v^2_W = (R_{tam}.\omega_{vc})^2 + (l.\dot{\gamma})^2 \quad (20)$$

Thus, the total kinetic energy of the system at the moment of impact is distributed into three parts:

$$KE = E_{cam} + E_{sway} + E_{diss} = \frac{1}{2} I_q.\omega^2_{vc} + \frac{1}{2} m_W (l.\dot{\gamma})^2 + \frac{1}{2} m_W (R_{tam}.\omega_{vc})^2 \quad (21)$$

According to the impulse theory in classical mechanics [5, 8], the quantity E_{diss} represents the portion of kinetic energy lost due to the imposition of an instantaneous constraint. When the cam stops abruptly, the radial velocity component $R_{tam}.\omega_{vc}$ of the counterweight - arising from the cam shaft rotation - is instantaneously eliminated by the constraint impulse at the shaft. The corresponding kinetic energy:

$$E_{diss} = (R_{tam}.\omega_{vc})^2.m_W/2 \quad (22)$$

3. IMPACT PHASE DYNAMIC MODEL

The hammer-head acceleration is the key parameter representing the impact load acting on the test specimen in Masset experiments. Due to the extremely short duration of the impact event and the harsh operating conditions, this acceleration cannot be measured directly using sensors [1, 6]. Therefore, it is determined indirectly from experimentally measured impact force combined with a dynamic model of the impact process. The cam-hammer system rotating about O is subjected to three moment contributions: the impact force $F(t)$ acting at the hammer head with lever arm R_b (the dominant excitation), the gravitational force acting at the center of mass G of the cam-hammer assembly, and the belt tension T_W acting at the contact point T. The rotational dynamic equation about O is given by:

$$I_q.\alpha(t) = M_{drive} - F(t).R_b - m_C.g.x_C - T_W.l_T \quad (23)$$

During the very short impact duration t_c, the cam rotation is negligible; therefore, the geometric quantities x_C and l_T, as well as the belt tension T_W, can be assumed approximately constant and taken at their values at the onset of impact [7], obtained from the dynamic simulation:

$$M_{static} = m_C.g.x_{C,vc} + T_{W,vc}.l_T \quad (24)$$

At the initial impact condition ($t = 0$, $F = 0$), the experimentally measured impact force is zero; therefore, the entire driving moment produces the angular acceleration corresponding to the known value obtained from the simulation results:

$$M_{drive} = I_q.\alpha_0 + M_{static} \quad (25)$$

Equation (23) can be rewritten as:

$$a(t) = R_b.\alpha(t) = R_b.\alpha_0 - F(t).R_b^2/I_q \quad (26)$$

The angular velocity of the system during impact is obtained by integrating the angular acceleration with respect to time [4]:

$$\omega(t) = \omega_0 + \int_0^t \alpha(\tau).d\tau = \omega_0 + \alpha_0.t - \frac{R_b}{I_q}\int_0^t F(\tau).d\tau = \omega_0 + \alpha_0.t - \frac{R_b}{I_q}J_T(t) \quad (27)$$

The angular velocity consists of two components: the free kinematic term $\int_{|0..t} \alpha_0.d\tau = \alpha_0.t$ and the impact impulse-induced term $(R_b/I_q).J_T(t)$. In practice, the hammer impact impulse J_T is composed of two parts: the measured component J_m (obtained from the experimental force curve) and the dissipated component J_{ls} (which cannot be directly measured). At the end of the impact phase, the system comes to a complete stop, i.e., $\omega_{(t=tc)} = 0$. From Eqquation (27):

$$J_T = (I_q/R_b)(\omega_0 + \alpha_0.t_c) \quad (28)$$

Let η denote the impulse absorption coefficient of the measurement structure; then:

$$\eta = J_m/J_T = J_m.R_b/[I_q.(\omega_0 + \alpha_0.t_c)] \quad (29)$$

It is assumed that the energy absorption ratio is approximately equal to the impulse absorption ratio during the impact phase: $E_m/E_{col} \approx J_m/J_T = \eta$. Substituting J_T into Eqquation (27) and applying the same procedure to the acceleration equation gives:

$$\omega(t) = \omega_0 + \alpha_0.t - \frac{R_b}{\eta I_q}J_m(t); \quad a(t) = R_b.\alpha_0 - \frac{R_b^2}{\eta I_q}F(t) \quad (30)$$

The total energy at the impact instant (used for validation when applying the parameter η) is given by:

$$E_{col} = E_{cam} + E_{drive} = \frac{1}{2}I_q\omega_{vc}^2 + I_q\alpha_0\int_0^t \omega(\tau)d\tau \text{ or } E_{col} = \frac{E_m}{\eta} = \frac{R_b}{\eta}\int_0^t F(\tau).\omega(\tau).d\tau \quad (31)$$

In this case, the energy absorbed by the sensor is:

$$E_m = R_b\int_0^t F(\tau)\omega(\tau)d\tau \quad (32)$$

and the dissipated energy (not absorbed by the sensor) is:

$$E_{ls} = E_{col} - E_m = (1-\eta).E_{col} \quad (33)$$

4. RESULTS AND DISCUSSION

After establishing the mathematical model of the system, the problem is solved following the sequence of motion phases. The rotational phase of the cam-hammer system is determined using Equations (12), (16), and system (17). The obtained results provide the initial conditions for the impact phase described by Equations (24) and (25).

4.1. Results of the rotational phase analysis

System (17): at $t = 0$, the cam starts from rest, with $\Delta\theta(0) = 0$, $\omega(0) = 0$, $\gamma(0) = 0$, $\dot{\gamma}(0) = 0$, L_d = 1.5 m; R_b = 1.2 m; m_C = 27.0 kg; m_W = 40.0 kg; R_C = 0.256 m; R_{tam} = 0.061 m; I_q = 1.843 kg.m^2.

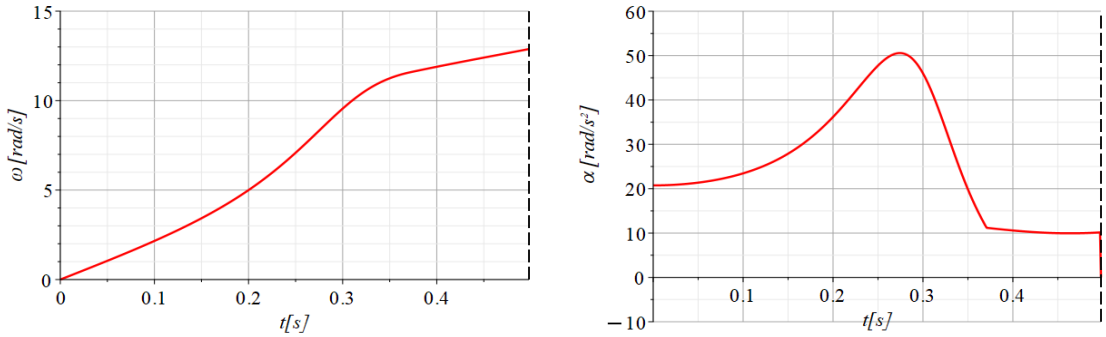


Figure 2. *Calculated angular velocity and angular acceleration prior to impact at tooth position 18.*

The computational results, from the moment the cam and hammer start moving at tooth position 18 until the hammer impacts the anvil (corresponding to a rotation of 199.5°), are shown in Figure 2. The results are verified based on the law of energy conservation.

At the moment of hammer–anvil impact, the total decrease in potential energy of the system ΔPE is 175.028 J, while the total kinetic energy ΔKE is 175.055 J, corresponding to an energy conservation error of 0.015%. The energy distribution at the impact instant shows that the kinetic energy is mainly concentrated in the cam-hammer motion, with a value of E_{cam} = 152.981 J (87.4%) (this quantity, E_{cam} is the cam-hammer kinetic energy exactly at the impact instant $t = 0$, and reappears in Section 4.2 as one component of E_{col}, the total energy at the impact instant used to validate η - see Equation 31), representing the effective impact energy transmitted to the anvil. The remaining E_{sway} = 9.719 J (5.6%) is stored in the oscillatory motion of the counterweight and does not directly contribute to impulse transmission. The instantaneous dissipated energy is E_{diss} = 12.354 J (7.1%), occurring at the instant of impact when the cam comes to an abrupt halt, causing the radial velocity component $R_{tam} \cdot \omega_{vc}$ of the counterweight to vanish instantaneously. The energy conservation error of 0.015% is well below 1%, confirming that the simulation results are reliable for engineering purposes.

4.2. Results of the impact phase analysis

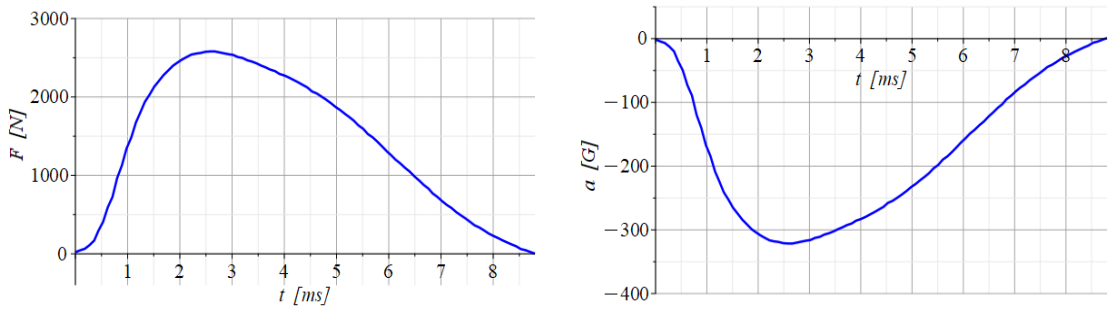


Figure 3. *Experimental and computed tangential acceleration after impact at tooth position 18.*

At the start of impact: ω_{vc} = 12.9 rad/s; α_{vc} = 10.15 rad/s^2. The impact force histories from four experimental tests (Figure 3a) show good convergence and are combined into a representative mean characteristic curve. The resulting acceleration profile is shown in Figure 3b. Other parameters are: E_{col} = 153.867 J; E_m = 97.981 J; E_{ls} = 55.886 J; maximum acceleration a_{max} = 321.4 G. The post-impact stopping condition $\omega(t=tc)$ = 0 is satisfied by construction, since η in Equation (29) is solved precisely to enforce this condition. Consequently, the impulse balance (Equation 28) and the energy balance (Equation 31) are analytical consequences of the same equation of motion rather than independent verification criteria; they serve as internal-consistency checks confirming that the numerical implementation is free of computational error (residual discrepancy ~10^{-4}%). The physical validity of the underlying assumption $E_m/E_{col} \approx J_m/J_T = \eta$ is supported indirectly by the fact that the resulting η (≈0.64) lies within a physically admissible range and is consistent with absorption ratios reported for comparable industrial hammer systems; direct independent verification (e.g., an auxiliary head-mounted accelerometer) is noted as a limitation and left for future work.

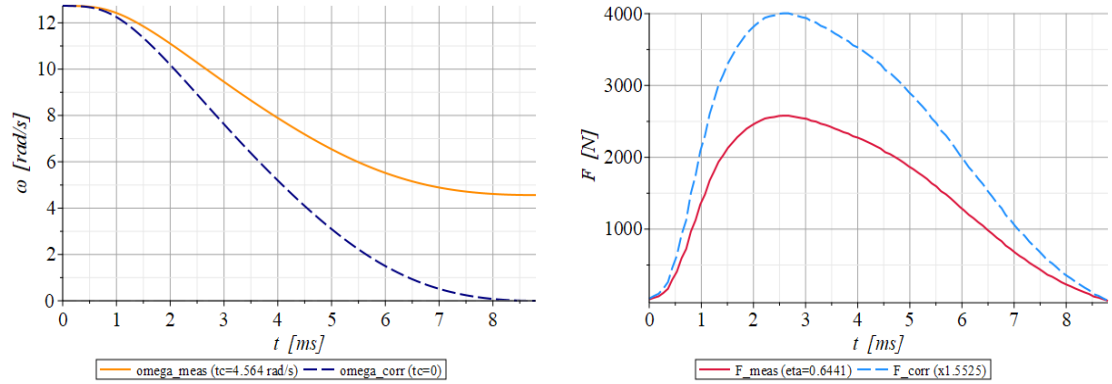


Figure 4. *Angular velocity and force during the collision process, considering the coefficient η.*

The coefficient η is introduced to ensure consistency between the calculated results and the actual parameters represented in the plots (Figure 4). The results show that 63.7% of the impact energy is transmitted to the anvil and recorded by the force sensor, while the remaining 36.3% is dissipated due to anvil absorption and contact deformation, consistent with values reported for similar industrial hammer systems.

5. CONCLUSIONS

This paper presents a method for determining the velocity and acceleration of a hammer during impact with an anvil. This is a challenging problem due to the extremely short impact duration (below 10 ms), the sudden, large-amplitude changes in acceleration, and the near impossibility of placing an accelerometer directly at the hammer head under severe impact conditions.

The core difficulty lies in the fact that the impact force measured at the anvil only represents part of the actual impulse acting on the hammer, while the remaining portion is dissipated within the anvil structure and contact zone and is not captured by the sensor. As a result, purely data-driven calculations from measured signals alone would not satisfy the physical requirement that the hammer must reach zero velocity at the end of the impact phase.

To address this issue, the proposed approach combines two complementary sources of information: the dynamic simulation provides the accurate state of the system at the impact instant, while the experimentally measured force history $F(t)$ describes the time evolution of the impact load. Based on this, the impulse absorption coefficient η is automatically identified to reconcile both data sources, ensuring consistency with the actual physical behavior.

The method is validated through three independent criteria and demonstrates high reliability.

Notably, it does not require material modeling in the contact zone or specialized sensors at the hammer head, making it suitable for analysis and design of similar Masset hammer systems.

REFERENCES

[1]. Ba Binh Phan, Van Yen Duong, "*Determining impact velocity in an impact tester using a mathematical model*", Journal of Science and Technique - Vol. 19, No. 03 (Nov. 2024).

[2]. "*Pyrotechnic Shock Testing*", Lesson 780, NASA LLIS, (1999)

[3]. CHEN. ZHIYONG, "*Pyroshock Testing of a Resonant Plate Using Hammer Impact*", POLITECNICO DI TORINO, (2023).

[4]. "*MIL-STD-810H*", Department of Defence, The United States of America, pp. 517.1-1 (2019).

[5]. H. Goldstein, C. Poole, J. Safko, "*Classical Mechanics (3rd Edition)*", Addison-Wesley, Chapter 10: Hamilton-Jacobi Theory and Advanced Topics in Analytical Mechanics, pp. 436-470, (2002).

[6]. J. J. Craig, "*Introduction to Robotics: Mechanics and Control*", Pearson Prentice Hall, pp. 45-78, (2005).

[7]. R. W. Ogden, "*Impact mechanics and energy dissipation in mechanical systems*", Proc. of 10th International Conference on Mechanical Engineering Dynamics, London, UK, pp. 112-118, (2010).

[8]. A. A. Deriglazov, "*Rigid Body as a Constrained System: Lagrangian and Hamiltonian Formalism*", Cambridge Scholars Publishing, ISBN: 978-1-0364-1287-6, (2024).

TÓM TẮT

Xây dựng phương pháp xác định các đặc trưng va chạm của búa Masset trên cơ sở kết hợp mô phỏng và thực nghiệm

Nghiên cứu này đề xuất phương pháp kết hợp giữa mô phỏng động lực học và số liệu thực nghiệm lực va đập nhằm xác định định lượng các đặc trưng động học của búa Masset trong toàn bộ quá trình làm việc, đặc biệt là gia tốc va đập - tham số khó xác định bằng thực nghiệm. Hệ số hấp thụ xung lực η được đề xuất để điều hòa quan hệ giữa lực đo tại đe và lực thực tế tác dụng lên búa, đảm bảo kết quả tính toán nhất quán với điều kiện vật lý thực tế. Kết quả cho thấy chỉ một phần năng lượng va chạm được truyền đến đe, phần còn lại tiêu tán do đặc tính hấp thụ của kết cấu - đây là cơ sở định lượng trực tiếp cho việc lựa chọn chế độ thử nghiệm. Phương pháp không yêu cầu mô hình vật liệu tại vùng tiếp xúc và có thể áp dụng cho các hệ thống búa tương tự.

Từ khoá: Búa Masset; Động lực học; Gia tốc va đập.